

# **Preliminary processing of physical modeling data from circular arrays**

David C. Henley

## **ABSTRACT**

Many novel transducer arrangements are possible for detecting and imaging targets in a physical modeling tank. We describe here some early developments in the processing used to extract useful target information from a physical model in which the acquisition geometry consists of a circular array of discrete receivers surrounding an unknown target, with sources regularly placed on the same circle as the receivers. Each source gather consists of recorded signals from all the receivers on the circular array accessible to that source, subject to the mechanical positioning limitations of the modeling system. Essentially, this experiment attempts to extract the 2-D shape of the object enclosed by the array, using principles of transit-time tomography and back-projection. Since target information in this experiment consists of variations of direct-arrival transit times from those expected for an empty circular array, our processing efforts are aimed at detecting those variations, projecting them as "shadows", and using various geometric processing tricks to combine the shadows in the processed source gathers to form a crude image of the target, for use as the starting point in an FWI procedure.

## **INTRODUCTION**

Physical modeling can be used to study many different problems where measurements of acoustic or elastic waves are used to obtain basic information about the object or target being investigated. The current physical modeling system developed and operated by CREWES has been used in many studies of elastic wave propagation suggested by various projects in the real world of seismic exploration, as well as those in wave propagation theory (Wong et al, 2016, Romahn and Innanen, 2017, Wong et al, 2019, Henley and Wong, 2019, Henley, 2020). In the present study, we exchange the environment of seismic exploration for that of medical imaging, with the hope that methods developed for seismic imaging can be used to enhance images used for medical diagnosis.

### **The medical diagnosis problem**

As we are all aware, the use of ultrasound to probe the human body and provide images of internal human organs is widespread; and has played a key role in the early diagnosis of many illnesses (Henley, 2021). Currently, ultrasound is mostly deployed in a backscatter, or reflection mode, and requires an experienced technologist to acquire and interpret the images, which are often diffuse and lack clarity. New research is aimed at using ultrasound not only in scattering mode, but also in transmission mode, to clarify and improve images of internal body structure. We expect that some techniques developed for use in Full Waveform Inversion may be applicable to producing high quality images from ultrasonic data, both scattering and transmission.

Traditional ultrasound uses a coincident source and receiver, which is applied to various locations on the surface of the body to form images of structures within the body. Because body tissues are very absorptive and don't differ very much in elastic properties, the

resulting images are sometimes faint and difficult to interpret. What we propose here is a different mode of imaging, in which an ultrasonic source radiates its energy into many receivers at different distances from the source, similar to the geometry used for X-rays in a CT scan. In a survey like this, not only will we obtain backscattered energy that can contribute directly to an image, but transmitted energy, as well, that can be used to provide tomographic images of transit time (‘time of flight’), or material absorption. Whereas backscattered energy contains mostly high frequency information about material boundaries, transmitted energy can provide measurements of material density and velocity of the volumes between the boundaries.

### Our experimental setup

The actual experimental setup for our work is described in more detail in Wong et al, 2021a and Wong et al, 2021b. Essentially, it consists of a circular array (scaled radius of 1200m or 1500m) of 72 positions where an ultrasonic transducer can be positioned in water in our modeling tank to act as a receiver. On the same circle are located 36 source positions where another transducer can be located to act as a source. Ideally, we would like to fire the source into the receiver at each of its 72 possible positions, for each unique source position, to provide a source gather consisting of 72 traces for each of the source positions. Practically, however, the fixtures on which the transducers are mounted must be prevented from colliding, which limits the accessible receiver positions for many sources. Instead of the 2592 recorded traces we would expect for fully accessible array positions, in reality, we obtain only 1331. Figure 1 shows the basic layout of the circle acquisition geometry.

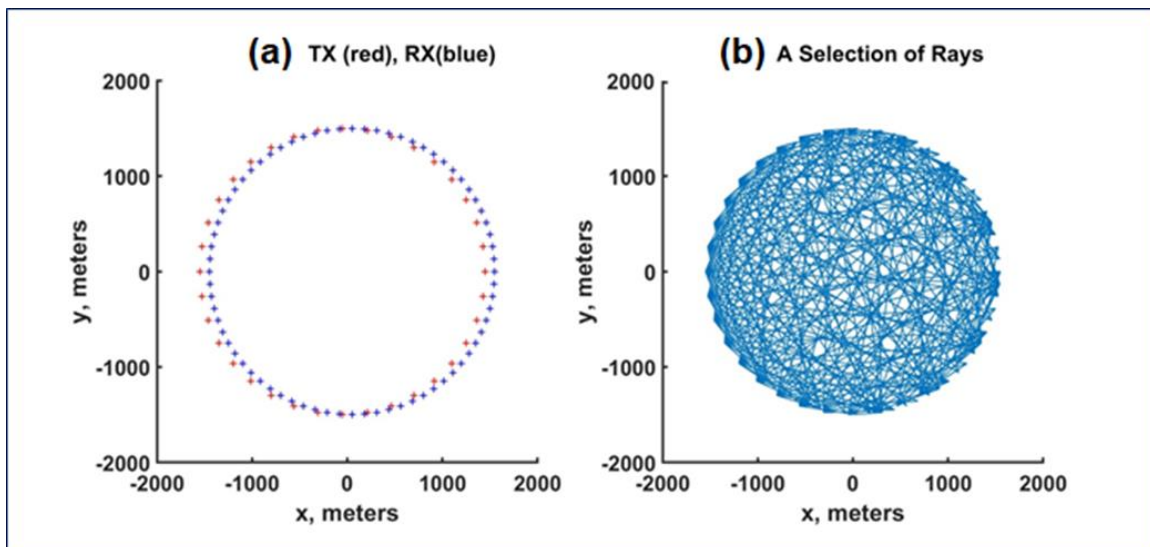


FIG. 1. (a) Schematic of acquisition geometry used for simulating the 1500m scaled radius physical model experiments. Note that there are 36 source positions (red), but twice as many receiver positions (blue), and that source and receiver can never be collocated due to the mechanical limitations of the acquisition apparatus. (b) A selection of possible rays along which acoustic energy can be transmitted. Not all these raypaths can be realized due to physical interference limitations of the acquisition apparatus. (Figure courtesy of Joe Wong).

For this experimental setup, we conduct two basic kinds of experiments; the ‘null’ experiment, where we simply acquire a full suite of source gathers in unobstructed pure

water, and the ‘target’ experiment, in which we place an object in the water somewhere inside the circumference of the acquisition circle and acquire a full suite of source gathers, which should then contain information about the intruding object. Although the acquisition geometry is strictly 2D, the geometry of any object placed inside the array is actually 3D, and we may expect some effects from this. Additional effects due to the radiation pattern of the transducers are expected to mainly affect arrival amplitudes. We do not attempt to deal with either effect in the present work.

### Goals for initial data analysis

Figures 2 and 3 show a group of source gathers of traces recorded with the described experimental setup; Figure 2 shows a portion of data for the 1500m circular array with no target present, while Figure 3 shows data from the same sources with a target placed somewhere inside the same 1500m array. We observe that the arrivals for the most direct raypaths can easily be seen, as well as other events at greater transit time, like the water surface multiple. While deeper data may contain backscattered information useful for imaging, we focused initially on the extraction of the transit times for energy arrivals along various raypaths, using various event picking techniques. Hence, we chose to devote our initial processing efforts to transit time analysis methods related to tomography and projection, hoping to develop a method for extracting an initial location and shape for a target. This image could then provide a starting point for FWI methods using backscattered radiation from the target (higher S/N for the circle acquisition waveforms will be required to achieve this goal).

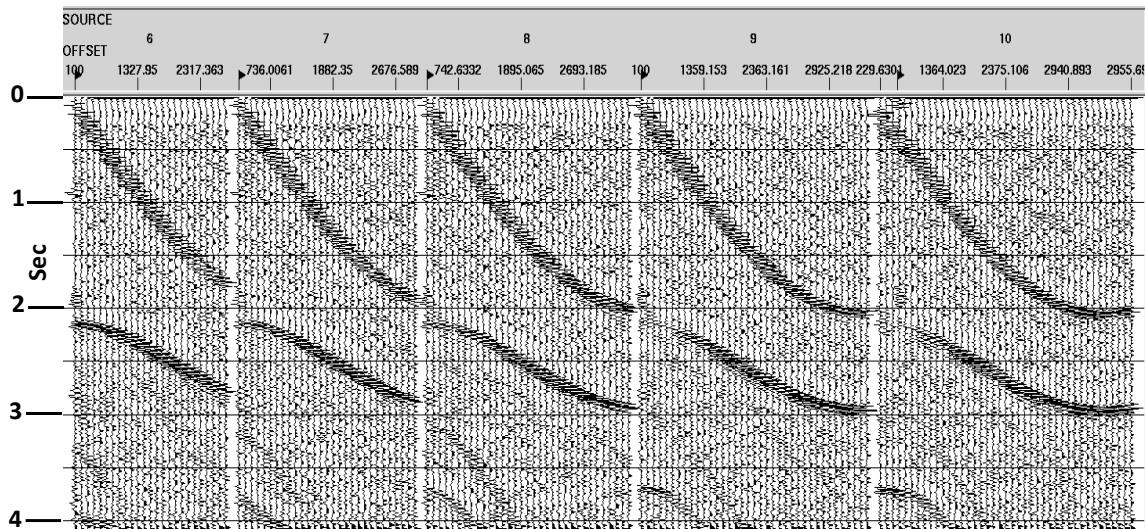


FIG. 2. Five recorded source gathers from the 1500m circle experiment, with no target present.

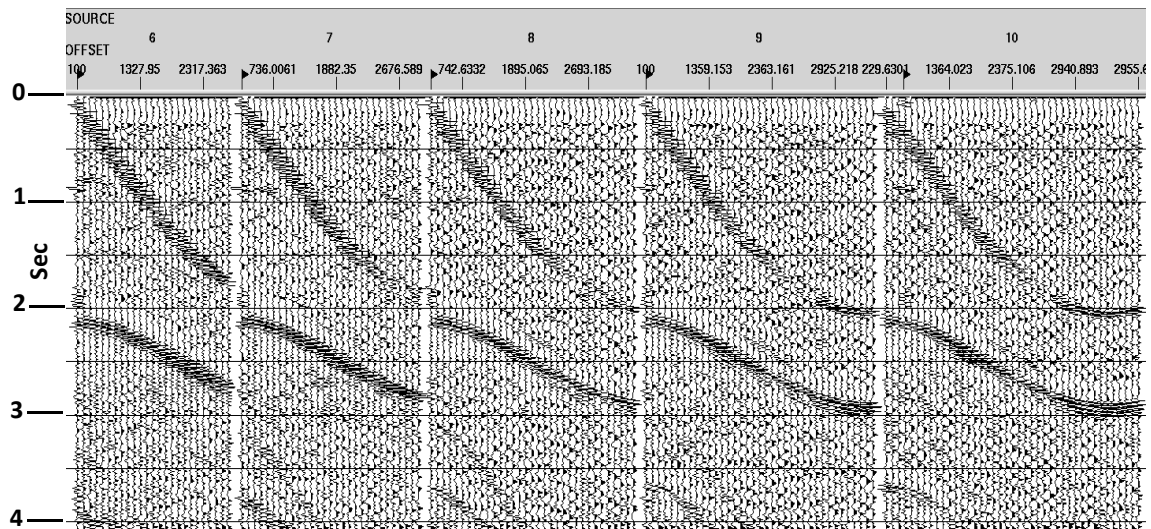


FIG. 3. Five recorded source gathers from the 1500m circle experiment, from the same source points as Figure 2, but with a PVC target present within the circular array. The presence of the target is revealed by the zones of diminished direct arrival amplitudes for source numbers 7-10.

## ANALYTIC PROCESSING OF CIRCLE ARRAY DATA

### Conventional processing

Since our goal in this first step of data analysis is to examine first arrivals, we first applied steps to make the data set more compact and amenable to visual examination. We know that the background medium of the model is water, so we first compute all the source-receiver offset values from the known  $x$  and  $y$  acquisition coordinates, then compute the transit time between each pair of source and receiver positions. These transit time values were stored in trace headers as 'vel\_stat', a static shift corresponding to the source-receiver time separation in water. When vel\_stat is applied to each trace as a static, the first arrival waveforms are roughly aligned, which allows the traces themselves to be truncated (we chose 500ms, and appended 100ms of blank trace ahead of the arrivals to make them easier to examine). To remove any jitter in the arrivals, due to slight transducer positioning errors, we applied a trim statics technique, with an aperture equal to the total number of traces in the data set. The result is the flattened event arrivals shown for three shot gathers in Figure 4. Note that the traces in each gather are sorted by source-receiver azimuth, and hence correspond to a 'fan' of raypaths from the source position to all receivers accessible from this source point. When we apply Gabor deconvolution and bandlimiting to sharpen arrival wavelets, we obtain Figure 5. One further step, necessary before any amplitude comparisons, is to compensate for spherical spreading, due to the different path-lengths for the traces spanning the circular array. After spherical spreading compensation, and a -20ms shift, the data are as shown in Figure 6.

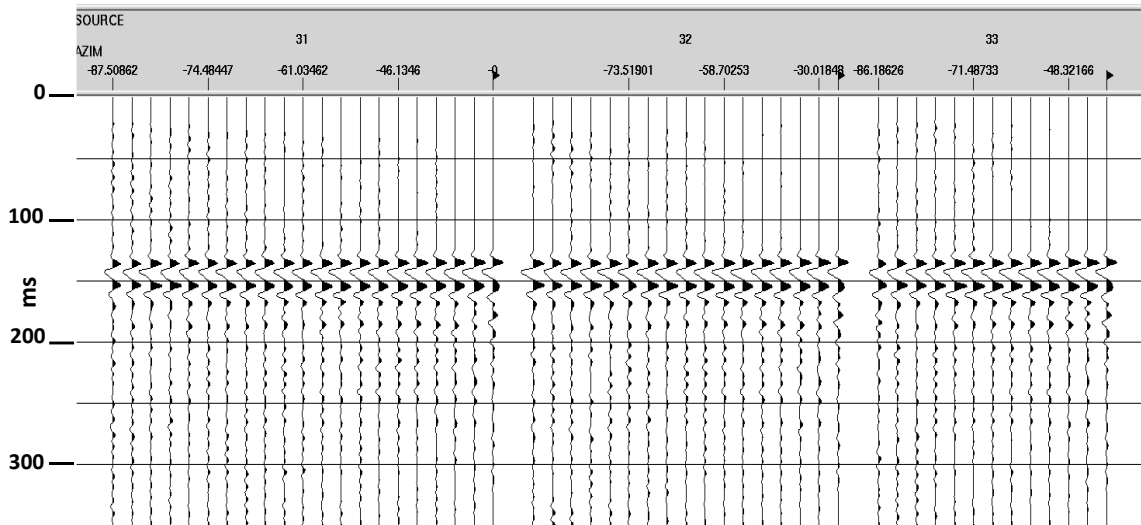


FIG. 4. Three source gathers from the 1500m circle experiment with no target present. These traces have been corrected for the transit time through water for the corresponding source-receiver offset, then aligned using a trim statics procedure which simultaneously used all the traces in the survey in the alignment window. The traces have all been shifted later in time by 120ms to better display the arrival waveforms, and an Ormsby bandpass filter of 2-4-110-150Hz applied.

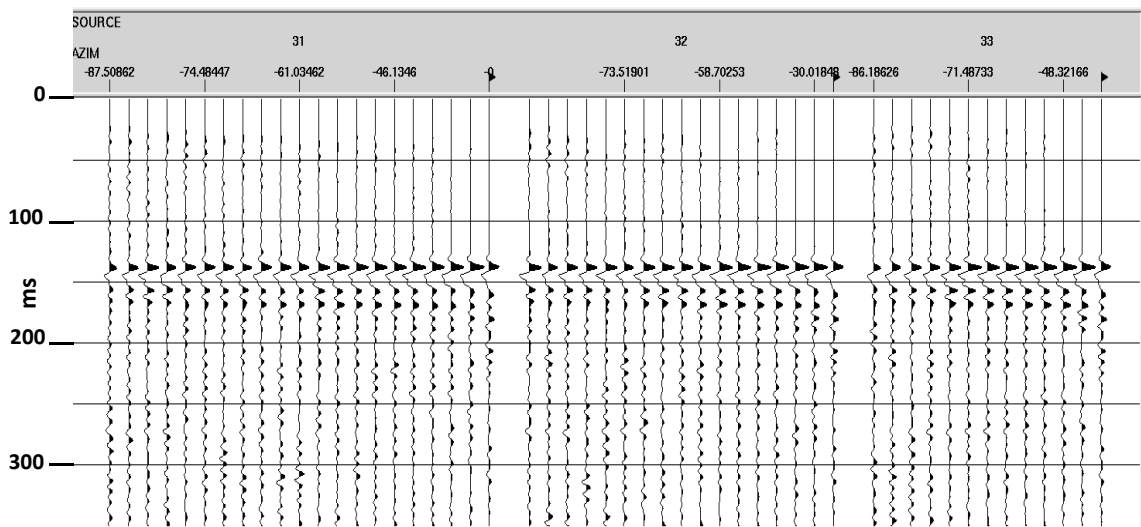


FIG. 5. The source gathers of Figure 4 after Gabor Deconvolution to whiten the spectrum and shorten the arrival wavelet. An Ormsby bandpass filter of 2-4-110-150 was applied.

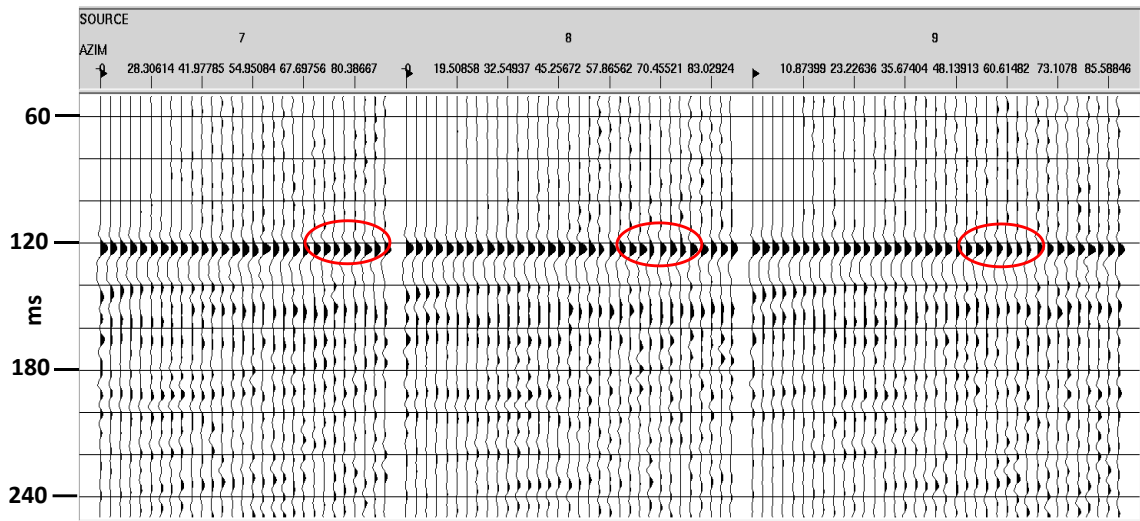


FIG. 6. Three source gathers from the 1500m no-target data set, after Gabor decon and amplitude compensation for spherical spreading.

So far, we have shown only data from the ‘null’ experiment, with no target inside the acquisition aperture. Figure 7, however, shows the same source gathers as Figure 6, but for the data set corresponding to the inclusion of a PVC target inside the acquisition circle. The amplitude differences are immediately apparent, with a ‘dim’ arrival zone appearing on each of the three shot gathers shown. Close examination shows some possible early arrivals above the dim zones, which we expect if the target is of higher velocity than the surrounding medium (water). We will examine these later. Figure 8 displays the amplitude differences between Figures 6 and 7. These amplitude differences can be thought of as crude projection images of the PVC target, where each projection conveys information primarily about the angular size of the target, but nothing about its thickness or distance from the source point. Since each shot sees the target from a slightly different angle, however, it should be possible, with some creative processing, to ‘triangulate’ the target projections, and perhaps rotate them into proper alignment to form a projection stack, or crude image of the object. Figure 9 illustrates this concept schematically.

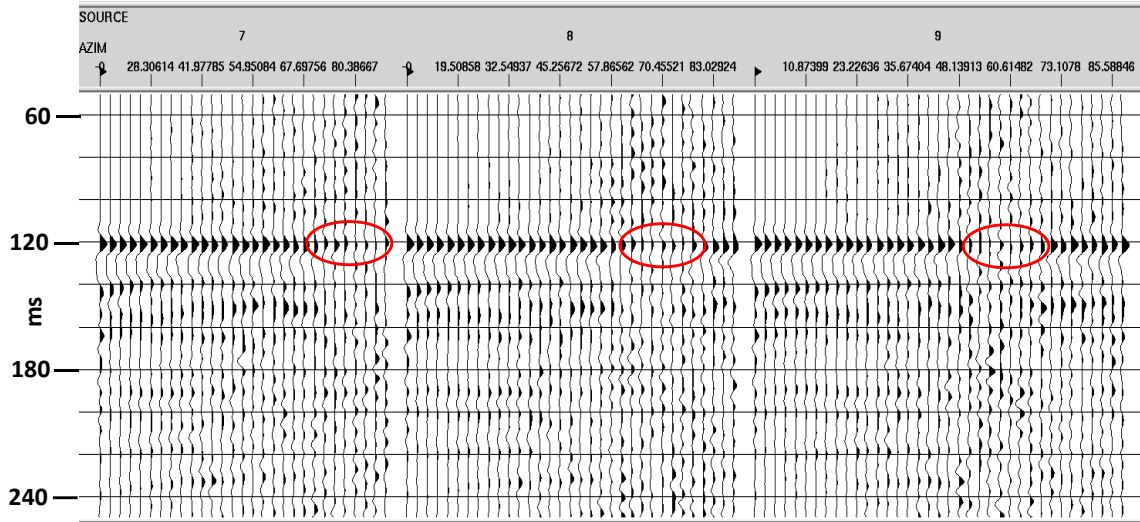


FIG. 7. Source gathers from the 1500m experiment with PVC target present. These gathers correspond to the ones shown in Figure 6, and they show the weak or missing arrivals from raypaths which encounter the target. The ovals in this figure can be compared with those in Figure 6. Since the source gather traces are arranged by source-receiver azimuth, the ovals indicate roughly how much angle the target object subtends from the source position for each source.

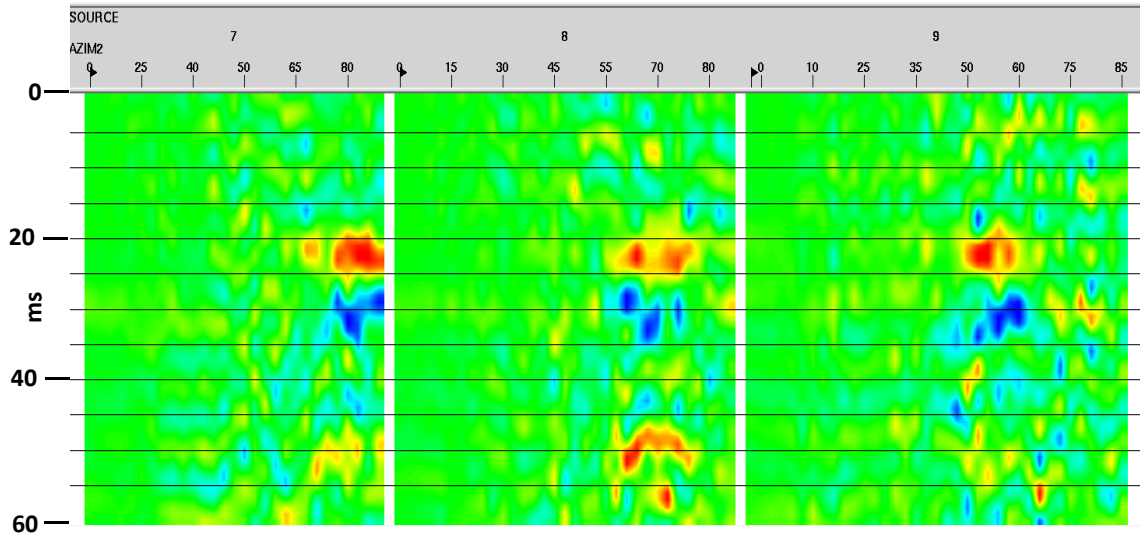


FIG. 8. Amplitude differences between source gathers in Figure 7 (with PVC target) and Figure 6 (no target). As in the previous figure, the subtended angular size of the object can be estimated from the 'azimuth' trace headers for each source gather.

Schematic for difference image geometry—Circle15 PVC minus Circle15  
 No Target—not exactly to scale

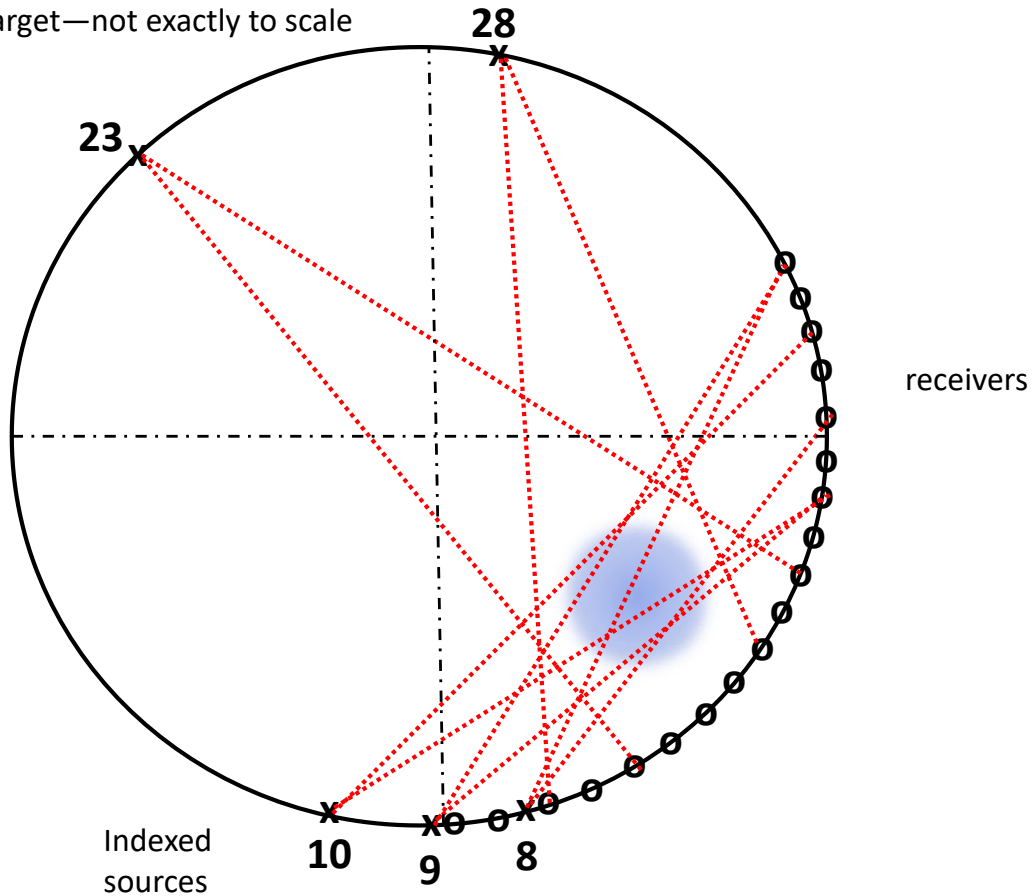


FIG. 9. Schematic showing the concept of triangulating the target object using sources whose trace gathers show a transit time anomaly or 'shadow' between azimuth limits.

**Creative processing**

To this point, we have shown and discussed the circle shooting data and their processing only in the conventional domain of seismic traces, which are time series recordings of the source wavelet as seen by the transducers located at each receiver location around the circular acquisition array. The most radical processing shown to date is the movement of the transmitted waveforms to a common transit time by the removal of the time delay due to transmission along straight raypaths through water, and the adjustment of the waveform transit times to a common time by means of a 'trim statics' procedure. This has allowed us to compare transmitted arrival wavelets, and to adjust their spectra and waveforms via Gabor deconvolution and bandpass filtering. We were able to display the amplitude anomaly between data recorded with the empty circular array, and data recorded in the presence of a PVC object located within the array, hence obtaining clues as to the physical location and size of the target object.

Next, we demonstrate some 'creative' processing techniques, in which we alter the amplitudes and coordinates of the recorded data according to strictly 'geometric' considerations, to allow us to apply particular transformations to the data, which lead, in

turn, to new ways to combine the modified data gathers into ‘shadow images’ showing the rough location and shape of the target object.

So far, we have displayed the data using coordinates of transit time, and either source-receiver offset, or source-receiver azimuth. We now consider arbitrary coordinates for the data amplitudes; in particular, substituting various algebraic formulae for computing source-receiver offset. These may have little or no relation to actual offset, but simply define the secondary coordinate of a current data matrix to enable us to use data transformation operations to remap the sample values geometrically.

*Forming the object shadows in the source gathers.*

Our goal for this stage of processing is to find the projected ‘shadows’ of the target object in each source gather and process the gathers appropriately for stacking them to create a ‘shadow image’ of the target relative to the circular array. The first part of our procedure is a non-linear process for creating shadows in the source gathers:

- We flattened the source gathers for the data set with object present, using the water-velocity static, plus trim statics with aperture equal to the total number of traces in the data set, resulting in source gathers like those shown in Figure 10. On these gathers, the anomalous arrivals are easily seen.
- We picked the anomalous arrivals seen on all source gathers and saved the picks as a horizon, Figure 11.
- We flattened the source gathers to the picked horizon, Figure 12.
- In a nonlinear step, we checked the ‘end of live samples’ trace header for each trace. For all traces where this trace header equals the originally set value, we set all trace amplitudes to zero. For any trace where the header value is larger than the original, we set all trace amplitudes to 1, tapering the amplitudes between top and bottom muting limits, hence creating a ‘shadow’. Figure 13 demonstrates the ‘shadows’ on several source gathers. At this point, the transit time coordinate of the traces becomes only a reference sample index.

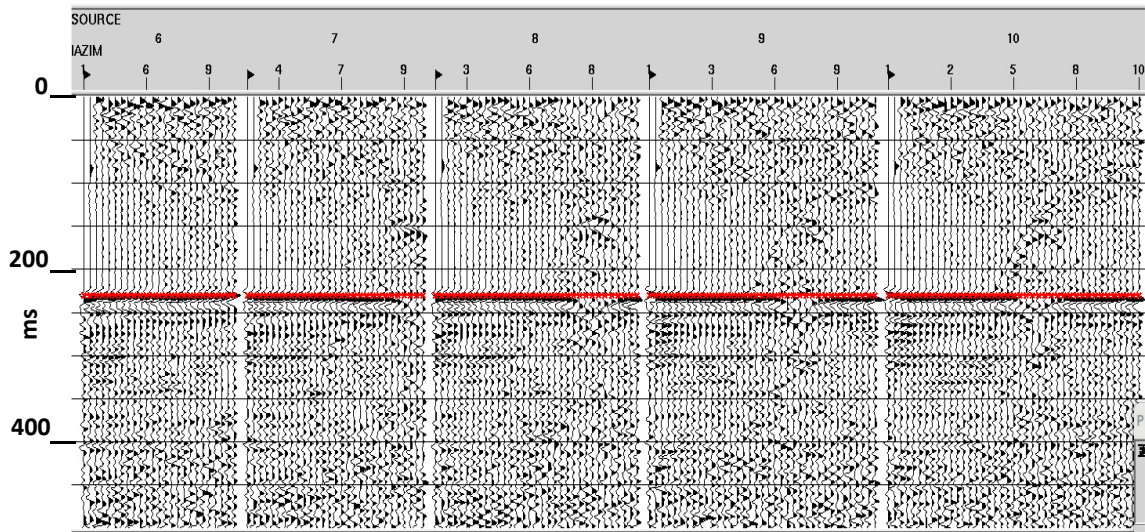


FIG.10. Five source gathers from the 1500m survey with PVC target; first arrival waveforms flattened to water velocity, aligned with trim statics procedure, Gabor deconvolved, amplitudes adjusted for spherical spreading, horizon picks for 1500m survey with no target overlaid in red.

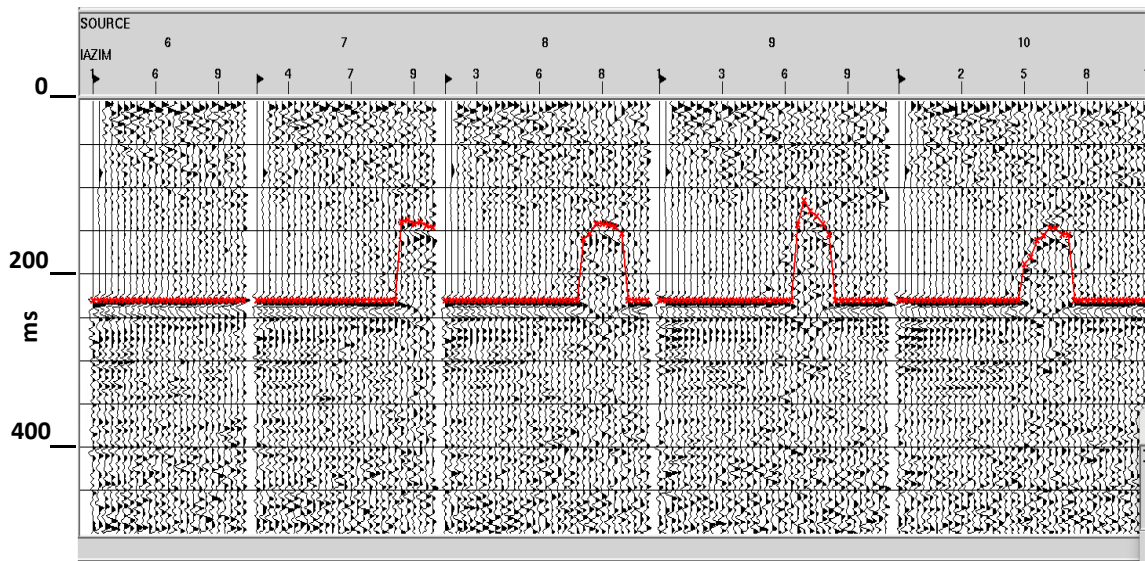


FIG. 11. Source gathers from Figure 10 with target arrivals picked as a horizon.

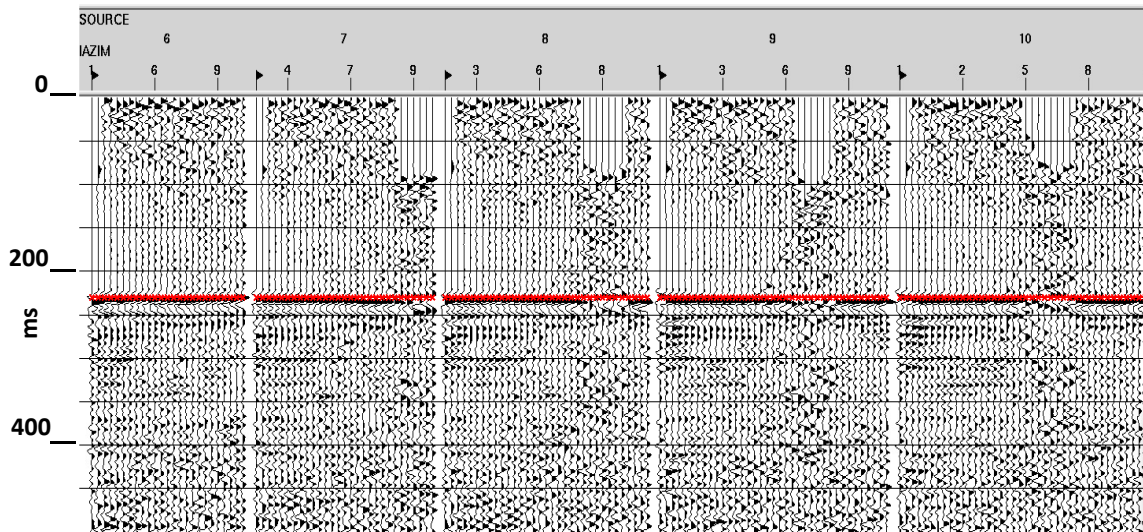


FIG. 12. Source gathers from Figure 10 flattened to the picked target horizon in Figure 11.

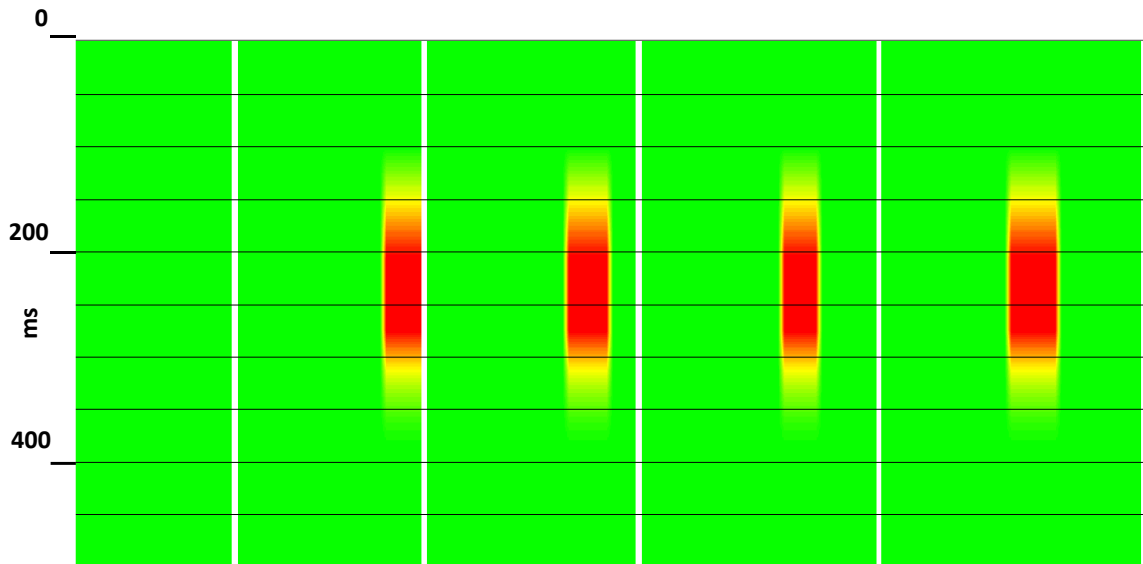


FIG. 13. "Shadows" created by sensing the flattened target events in Figures 10 and 11. The shadows are centred on the flattened event times and tapered above and below.

### *Manipulating the object shadows*

As shown in Figure 13, the projection shadows for the target are oriented vertically in each source gather, where the primary coordinate is source-receiver azimuth. The shadow in each source gather is bounded by azimuth limits, which are different for each source gather, but may overlap. Confounding the issue is the fact that each source point around the circumference of the circular array illuminates the accessible receivers at different azimuths; hence stacks of traces from the original acquisition domain are not appropriate. We need to rotate each source gather in some fashion so that its raypaths are properly oriented relative to those of other source gathers and can be stacked appropriately.

We know of two simple re-mapping operations that can be applied to 2D seismic trace panels to rotate their sample values to new coordinates; the Radial Trace Transform (Henley, 1999a, Henley, 1999b, and Henley, 2011) and Linear Moveout correction. Both require the signed source-receiver offset trace header; but we can define this header any way we like, to create the geometrical relationship desired. For both operations, we ignore the original purpose, and use the header value as a parameter to re-map data arrays.

In the case of the Radial Trace Transform, amplitudes are re-mapped from the original domain of primary trace coordinate and transit time to a new domain of slope, or ray parameter and transit time. The sampling trajectory slopes can be chosen to span a wide range of ray parameters or velocities (RT fan transform), or to isolate a single predominant slope (RT dip transform). In our current application, we choose the RT dip transform with the slope velocity as a user parameter, which can be chosen according to the ‘offset’ trace headers in the source gathers (which can be generated using any formula desired, as long as offsets monotonically increase with trace number in a gather) As can be seen in Figure 14, applying an RT dip transform with nominal velocity of -4000m/sec leads to trace panels in which the projection shadows are tilted relative to the coordinate axes.

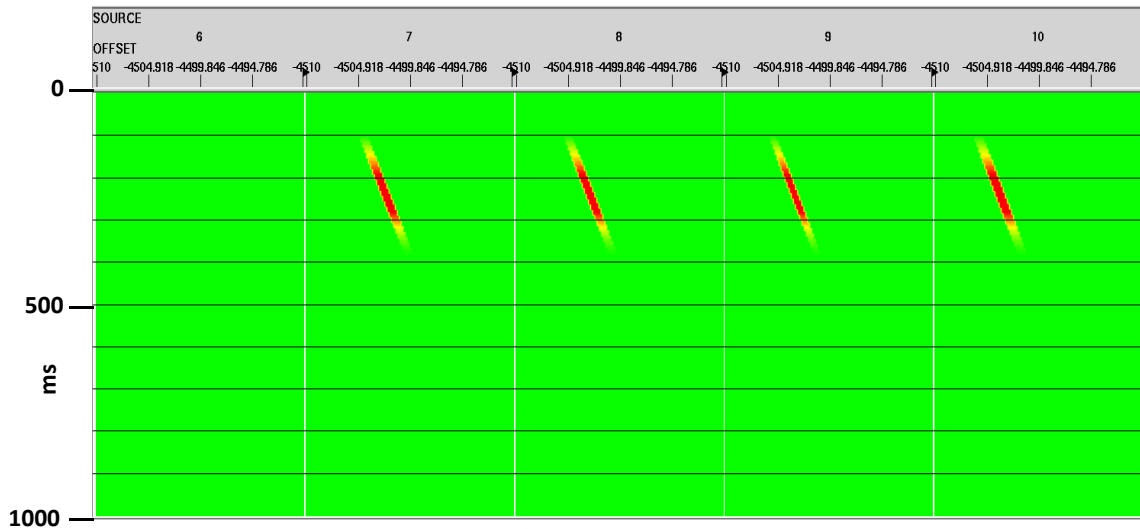


FIG. 14. RT Dip Transform,  $V = -4000\text{m/s}$ , applied to “shadow” source gathers in Figure 13 to rotate the shadows.

The Linear Moveout transform applies time shifts to seismic traces that are proportional to the ‘offset’ header in each trace, with the velocity parameter in the LMO operation determining the trace shift relative to its posted offset value. The previous RT transform destroys the original offset values in the trace headers, so we are free at this point to create any set of headers that will help orient the shadows during the LMO. After considerable experimentation, we determined that an offset formula with increment based on the trace sequence number within a source gather, scaled by the sum of the source-receiver azimuth and the azimuth of the source from the circular array centre, provides the desired angular rotation of each shadow within its 2D source array. An adjustable scalar factor can be used to ensure that the sum of the rotations of the visible shadows do not exceed the fraction of

the maximum 360deg circular aperture viewed by the source gathers containing visible shadows. See Figures 15, 16, and 17.

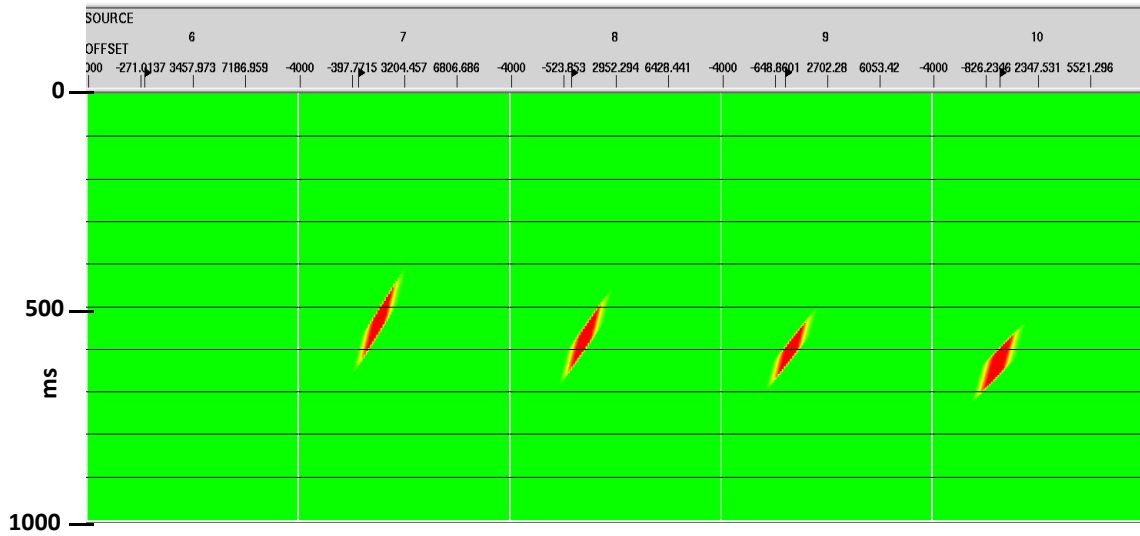


FIG. 15. Shadows tilted by RT Dip Transform and rotated by LMO, with bulk shift also applied.

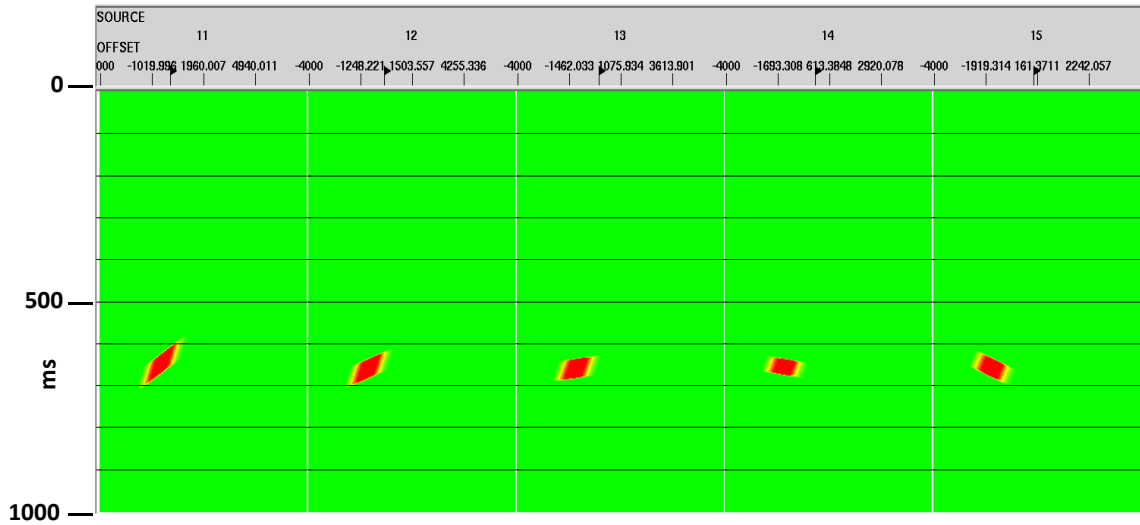


FIG. 16. Shadows tilted by RT Dip transform and rotated by LMO, with bulk shift also applied.

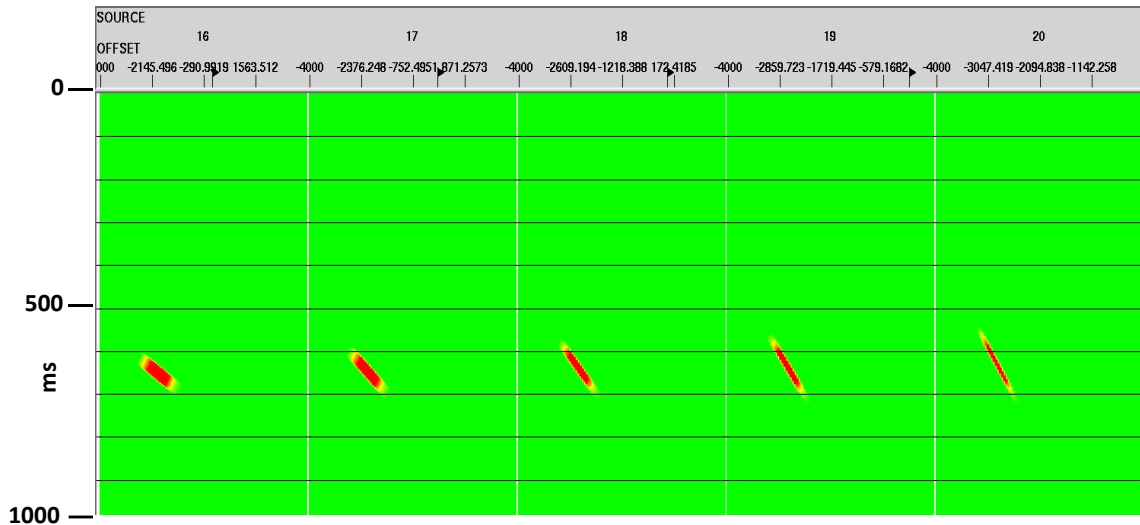


FIG. 17. Shadows tilted by RT Dip transform and rotated by LMO, with bulk shift also applied.

Although the desired shadow rotations are applied by the LMO acting on appropriate offset headers, the rotated shadows need to be adjusted in time index to stack appropriately. An additional formula creates a source number dependent static shift that can be used to align the shadows in time as shown in Figure 18. The variation in time index as a function of source gather number seen in the shadow positions within the source gathers is almost certainly a reflection of the fact that the object casting the shadows is offset some distance from the boundary of the circular receiver array. How to interpret this variation remains to be addressed.

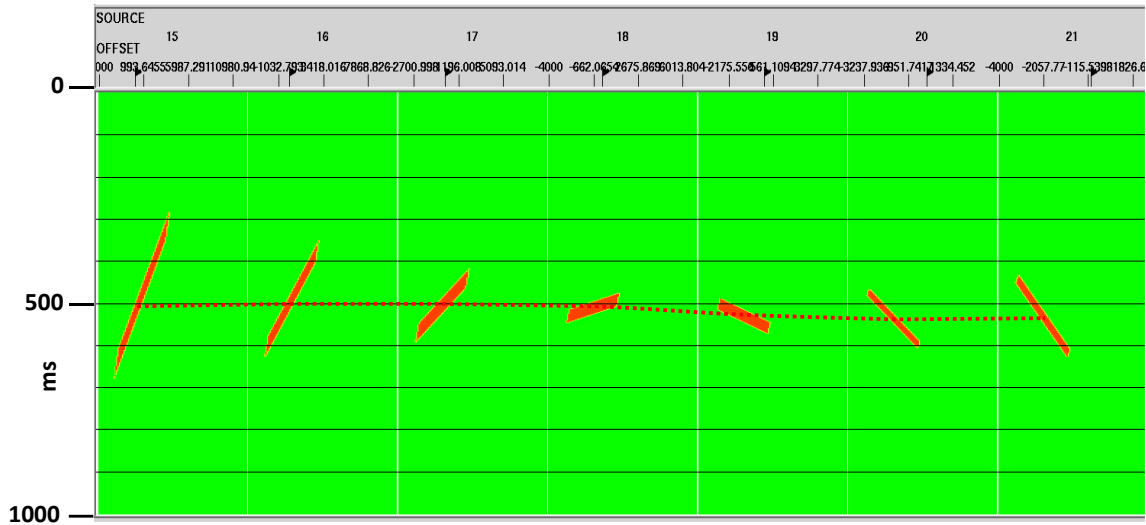


FIG. 18. Tilted shadows shown with alignment provided by LMO.

*Comments*

The transmission data acquired from a survey using a circular array of receivers with sources located on the receiver circle are originally presented as source gathers, which

means that geometrically, each represents a ‘fan’ of raypaths. We process these data by removing the raypath length via a water-velocity-based static correction; and associate the source-receiver azimuth with each compensated data trace. Seismic arrivals deviating in transit time from the signals on these compensated traces are assumed to have encountered a ‘target’ object before impinging on their respective receivers. Since each source gather ‘sees’ the target from a slightly different angle (if at all), the projected angles of the target ‘shadow’ can be used to roughly locate the target and estimate its size, when all projected shadows are rotated to the same reference frame and stacked. The procedure for stacking and displaying the data remains uncertain, particularly since the desired image needs to be displayed in cartesian coordinates scaled to the acquisition geometry frame. The desired image geometry is as shown schematically in Figure 9.

Figure 19 is our best attempt at stacking the rotated and aligned shadows from the transmission survey. The CDP coordinate shown is just an index value computed from the source number and receiver number, and thus related to their midpoint. An attempt to incorporate the survey geometry in a more exact way constitutes ongoing research. Figure 19 is shown here simply to illustrate our objective. Ultimately, we expect to display a shadow stack similar to Figure 19, but with cartesian coordinates derived from the original survey geometry.

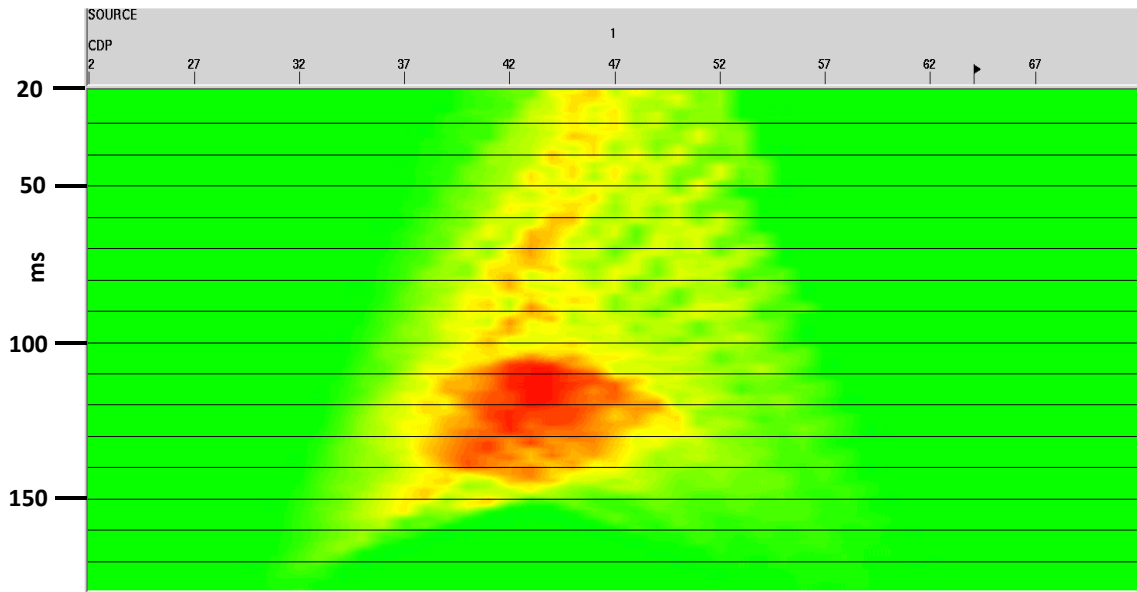


FIG. 19. Trial stack of projection shadows from circle15 transmission survey. Geometry needs to be invoked to change coordinates of CDP and transit time to cartesian coordinates of position.

## DISCUSSION

As we stated at the outset, our objective in this study was to use only the information available to us in transmission seismic data; hence we have examined only the first arrivals of the circular array acquisition data measured in the physical modeling tank, and we have demonstrated our processing ideas only on the data set from the circular array with scaled radius of 1500m.

Had we chosen a traditional tomographic approach to these data, we would have picked all the first arrivals and submitted them to a tomographic inversion algorithm, like back-projection. This may still prove to be the best way to obtain a first approximation of the image of a target, but we decided to explore a different idea in this study. We approximated the first arrival picking by computing transit times from source-receiver offset distances and water velocity, then adjusting these with a trim statics procedure. The only first arrivals that were hand picked were those that deviated from the water velocity due to the embedded PVC target. As seen in Figures 10 and 11, these arrivals were relatively easy to find and pick, and were posted in combination with the trim-statics-adjusted water-velocity statics as a horizon, to which the source gathers for the survey could be flattened, as in Figure 12. This procedure makes it easy to construct a data set consisting of zero traces and “shadows”, simply by monitoring the trace headers which track the last valid data sample for each trace. Each shadow in a source gather indicates which traces in a source gather have encountered the target before arriving at a receiver, and it flags the source-receiver azimuth for those traces. On an individual gather, however, the shadow gives no indication of the position of the target along the transit path. This information is only obtainable from triangulating the shadows from two or more source gathers.

Our idea for triangulating the shadow gathers is based on rotating the gathers relative to each other, based on the azimuth of each source from the origin of the circular array, then stacking their shadows. The rotation of these gathers is not trivial, since their coordinates are source-receiver offset (or source-receiver azimuth, or recording channel) and transit time. Coordinate rotation of these data involves at least one re-sampling operation; we chose the Radial Trace Dip transform, which re-samples a seismic gather along constant velocity trajectories through the original gather. After transforming the data to a velocity (ray-parameter) domain, further rotation can be applied using the linear moveout (LMO) operation. We chose this option, rather than applying a separate RT Transform to each source gather. Furthermore, we can scale the LMO operation by re-setting the offset headers of the source gather traces with each new source gather. In this way, we can ensure that the shadow rotation applied to a set of source gathers covering a complete circular array does not exceed 360deg.

At this point, we have demonstrated the mechanics of our processing flow; but details remain to be explored.

## ACKNOWLEDGEMENTS

We acknowledge funding from CREWES sponsors and NSERC, and the use of seismic software contributed by Halliburton.

Discussions with Joe Wong and Kris Innanen provided insight and are gratefully acknowledged (even though seemingly ignored at times).

## REFERENCES

- Henley, D.C., 1999a, Coherent noise attenuation in the radial trace domain: introduction and demonstration: *CREWES Research Report*, **11**, 36, 37.
- Henley, D.C., 1999b, Demonstration of radial trace domain filtering on the Shaganappi 1998 2-D geotechnical survey: *CREWES Research Report*, **11**, 58, 17.
- Henley, D.C., 2011, Now you see it, now you don't: radial trace filtering tutorial: *CREWES Research Report*, **23**, 44, 25.
- Henley, D. C., and Wong, J., 2019, Let there be light: illuminating physical models from the surface: *CREWES Research Report*, **31**, 22, 27.
- Henley, D. C., 2020, A tale of two realities; reconciling physical and numerical modeling via 'bootstrap' processing: *CREWES Research Report*, **32**, 23, 28.
- Henley, D.C., 2021, Personal note: In July 2021, the experienced analysis of an abdominal ultrasound session by an alert physician at the imaging laboratory sent me to the emergency room for emergency gallbladder surgery, and other procedures, that likely prevented me from experiencing rather serious consequences.
- Romahn, S. J., and Innanen, K. A. H., 2017, The seismic physical modelling laboratory as a tool for design and appraisal of FWI methods: *CREWES Research Report*, **29**, 66, 22.
- Wong, J., Bertram, K. L., and Hall, K. W., 2016, Physically-modeled 3D surveys over a channel structure: *CREWES Research Report*, **28**, 79, 8.
- Wong, J., Zhang, H., Kazemi, N., Bertram, K. L., Innanen, K. A. H., and Shor, R., 2019, Physical modeling of seismic illumination and SWD: *CREWES Research Report*, **31**, 53, 14.
- Wong, J., Bertram, K. L., and Innanen, K. A. H., 2021a, Acquiring physically-modeled seismic data using 70kHz piezoelectric buzzers, **33**, 46.
- Wong, J., Henley, D. C., and Innanen, K. A. H., 2021b, Analyzing buzzer-acquired physical model data for FWI, **33**, 47.